ORGANOMETALLICS
Article
pubs.acs.org/Organometallics

Investigations of the Electronic Structure of Arene-Bridged Diuranium Complexes

Bess Vlaisavljevich,[†] Paula L. Diaconescu,*[,‡] Wayne L. Lukens, Jr.,*[,§] Laura Gagliardi,*[,†] and Christopher C. Cummins*[,∥]

[†]Department of Chemistry, Supercomputing Institute, and Chemical Theory Center, University of Minnesota, Minneapolis, Minnesota 55455, United States
[‡]Department of Chemistry & Biochemistry, University of California, Los Angeles, California 90095, United States
[§]Chemical Sciences Division, Lawrence Berkeley National Laboratory, Berkeley, California 94720, United States
[∥]Department of Chemistry, Massachusetts Institute of Technology, Cambridge, Massachusetts 02139, United States

S *Supporting Information*

ABSTRACT: The electronic structure of the arene-bridged complex (μ-toluene)U_2(N[^{t}Bu]Ar)$_4$ (**1a**$_2$-μ-toluene, Ar = 3,5-$C_6H_3Me_2$) has been studied in relation to a variety of mononuclear uranium amide complexes, and their properties have been discussed comparatively. The syntheses, molecular structures (X-ray crystal structures and solution behavior based on variable-temperature NMR spectroscopic data), and corresponding spectroscopic (X-ray absorption near-edge structure and UV−vis−near-IR absorption) and magnetic properties are presented and interpreted with reference to results of density functional theory (DFT) and complete active space self-consistent field with corrections from second-order perturbation theory (CASSCF/CASPT2) calculations performed on model compounds. While the mononuclear compounds display expected electronic and magnetic properties for uranium complexes, **1a**$_2$-μ-toluene shows complicated properties in contrast. XANES spectroscopy, X-ray crystallography, and both density functional and CASSCF/CASPT2 results are consistent with the following electronic structure interpretation: f orbitals host the unpaired electrons, followed energetically by two δ bonds formed by filled uranium f orbitals and LUMOs of toluene.

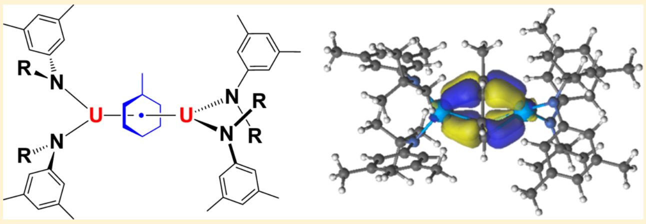

■ INTRODUCTION

Arene-bridged complexes constitute a general bonding motif for organouranium compounds featuring benzene/toluene,[1−9] naphthalene,[10] biphenyl,[11] cycloheptatrienyl,[12,13] or cyclooctatetraene[10] as the bridging arene ligand. In most cases, as well as in actinocene complexes, δ bonding[14] between f orbitals of uranium and ligand LUMOs (lowest unoccupied molecular orbitals) of the appropriate symmetry is considered to play a major role.[1,2,5] Like π bonding in transition-metal chemistry, δ bonding may be key to understanding uranium complexes; however, the electronic structures of arene-bridged diuranium complexes have rarely been investigated beyond the usual techniques.[2,5]

Amide ligands have become ubiquitous in transition-metal chemistry,[15−17] and they also proved successful in supporting interesting actinide complexes.[6,18−30] Their versatility is largely based on the tunability of electronic and steric properties that takes advantage of the ability to modify the two substituents of the nitrogen donor.[15,31] These properties allowed the isolation and characterization of arene-bridged diuranium complexes in which the arene is either toluene or benzene.[1]

The focus of this report is to investigate the electronic structure of the arene-bridged complex (μ-toluene)U_2(N[^{t}Bu]-Ar)$_4$ (**1a**$_2$-μ-toluene, Ar = 3,5-$C_6H_3Me_2$) by comparison with the mononuclear complexes (THF)U(N[Ad]Ar)$_3$ (**2b**-THF, Ad = 1-adamantyl, THF = tetrahydrofuran), IU(N[^{t}Bu]Ar)$_3$ (**2a**-I), IU(N[Ad]Ar)$_3$ (**2b**-I), and (Me_3SiN)U(N[Ad]Ar)$_3$ (**2b**-NSiMe$_3$), such that a range of uranium formal oxidation states is surveyed. In order to understand the properties of a unique compound such as **1a**$_2$-μ-toluene, the rest of the series is based on classical uranium amide compounds, for which there is no ambiguity about the oxidation state. The syntheses, molecular structures (X-ray crystal structures and solution behavior based on variable-temperature NMR spectroscopic data), and corresponding spectroscopic (X-ray absorption near-edge structure and UV−vis−near-IR absorption) and magnetic properties are discussed and interpreted with reference to results of computational studies performed on model compounds; X-ray absorption near-edge structure (XANES) spectroscopic characterization of arene-bridged diuranium complexes has not been reported previously.

Special Issue: Recent Advances in Organo-f-Element Chemistry

Received: November 1, 2012
Published: February 20, 2013

dx.doi.org/10.1021/om3010367 | *Organometallics* 2013, 32, 1341−1352

RESULTS AND DISCUSSION

Syntheses and X-ray Crystal Structures. The synthesis of compound $\mathbf{1a}_2$-μ-toluene and the X-ray crystal structure of the related (μ-toluene)$U_2(N[Ad]Ar)_4$ ($\mathbf{1b}_2$-μ-toluene) as well as reactivity studies have been reported previously.[1] Scheme 1 describes the syntheses of all the complexes discussed here. $UI_3(THF)_4$[32,33] is a versatile starting material and can be employed to obtain tris(amido)uranium iodide complexes **2a**-I and **2b**-I or can be used to generate $\mathbf{1a}_2$-μ-toluene and **2b**-THF directly. In general, compounds based on the *N-tert*-butylanilide ligand are more lipophilic and, in practice, are less crystalline than compounds based on the *N*-adamantylanilide ligand.

Scheme 1. Syntheses of Uranium Complexes Discussed in the Text

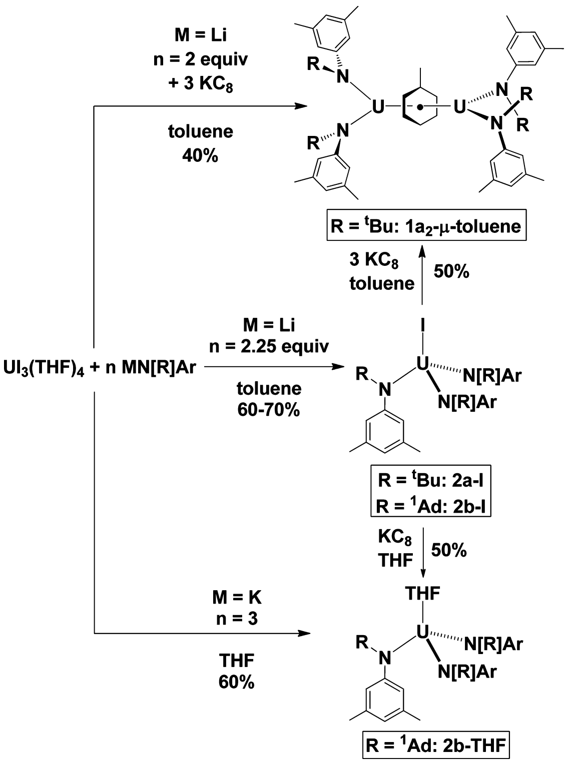

Reduction of the tris(amido)uranium iodide compounds affords either arene-bridged diuranium complexes, when the arene is used as a solvent,[1] or uranium tris(amide) complexes with a molecule of THF coordinated to the uranium center, when THF is used as a solvent.[21] Finally, **2b**-$NSiMe_3$ is obtained from the reaction of Me_3SiN_3 with **2b**-THF, which can be generated in situ or isolated prior to the reaction (eq 1).

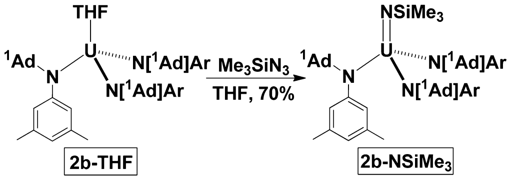

(1)

The formulation of these compounds was verified by X-ray crystallography (Figures 1−3). A metrical parameter present throughout the entire series is the distance $U-N_{amide}$(av). This distance of 2.334(13) Å in $\mathbf{1b}_2$-μ-toluene is slightly shorter than the 2.346(9) Å found for **2b**-THF (Figure 1); both values are ca. 0.1 Å longer than the corresponding distances in **2b**-I (Figure 2) and **2b**-$NSiMe_3$ (Figure 3), at 2.204(9) and 2.245(7) Å, respectively. The trend observed here is in good agreement with the results of XANES experiments (see below), which show that the effective charges on the uranium center are similar for $\mathbf{1a}_2$-μ-toluene and uranium(III) compounds, on one hand, and for **2b**-I and **2b**-$NSiMe_3$, on the other hand.

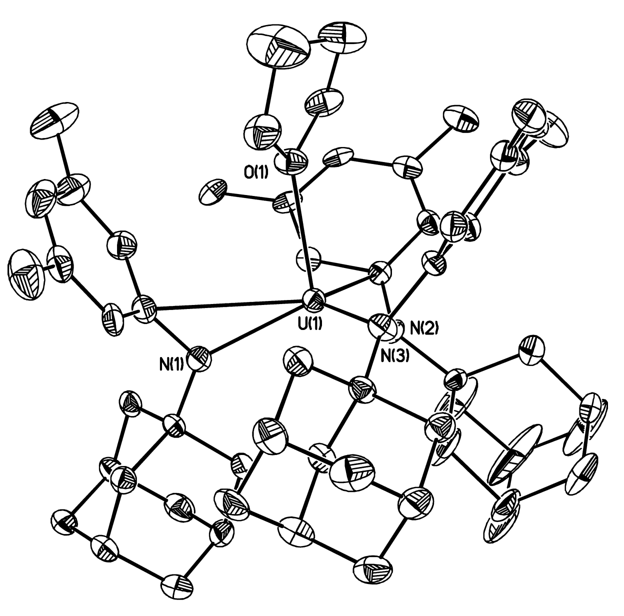

Figure 1. Structural drawing of **2b**-THF with thermal ellipsoids at the 35% probability level and hydrogen atoms omitted for clarity. Selected distances (Å): U−N(av), 2.346(9); U−O, 2.489(5).

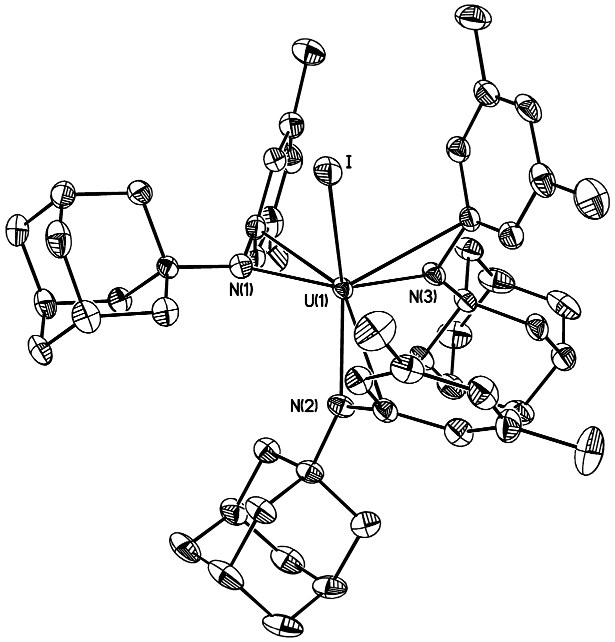

Figure 2. Structural drawing of **2b**-I with thermal ellipsoids at the 35% probability level and hydrogen atoms omitted for clarity. Selected distances (Å): U−N(av), 2.204(9); U−I, 3.0682(4).

The structure of **2b**-$NSiMe_3$ (Figure 3) distinguishes itself by the $U-N_{imide}$ distance of 1.943(4) Å, which is ca. 0.3 Å shorter than the average $U-N_{amide}$ distance (2.245(7) Å) in the same compound. Short $U-N_{imide}$ distances and angles close to 180° at N_{imide} (170.1(13)° in **2b**-$NSiMe_3$) have been associated with

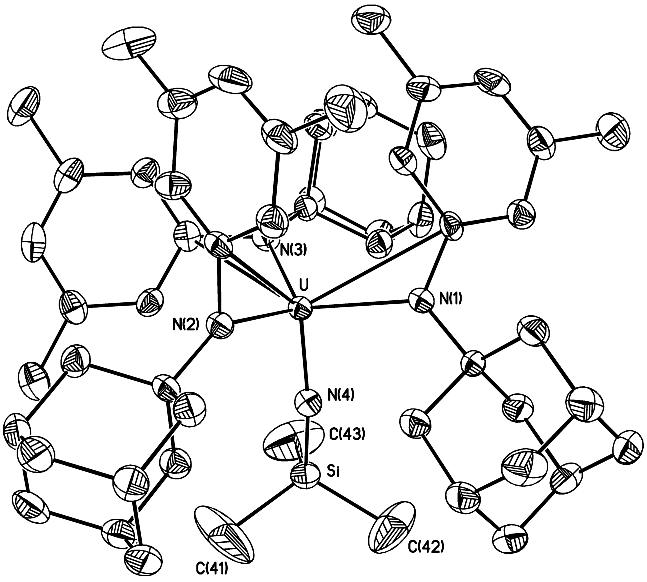

Figure 3. Structural drawing of **2b**-NSiMe$_3$ with thermal ellipsoids at the 35% probability level and hydrogen atoms omitted for clarity. Selected distances (Å): U−N$_{amide}$(av), 2.245(7); U−N$_{imide}$, 1.943(4).

multiple-bond character between the uranium center and the imide nitrogen atom,[34] in accordance with our findings from CASSCF calculations on a model compound (see Computational Results).

The structure of **1b**$_2$-μ-toluene features an average distance of 2.594(30) Å between uranium and the carbon atoms of the bridging toluene molecule that is similar to those in other toluene- or benzene-bridged diuranium complexes.[2,5] These values are among the shortest such distances registered for carbon atoms of arenes coordinated to uranium centers. For example, the average U−C distance is 2.647(10) Å in uranocene, U(η^8-C$_8$H$_8$)$_2$,[35] and 2.807(18) Å in U(η^5-C$_5$H$_5$)$_4$,[36] while in benzene complexes such as U(η^6-C$_6$Me$_6$)(BH$_4$)$_3$[37] and U(η^6-C$_6$H$_5$Me)(AlCl$_4$)$_3$,[38] the average U−C distance is significantly longer: 2.93(2) and 2.94(1) Å, respectively. The average C−C distance of 1.438(13) Å for the bridging toluene in **1b**$_2$-μ-toluene is ca. 0.04 Å longer than the corresponding distances in free toluene.[39] In complexes of toluene such as K(18-crown-6)(toluene),[40] C−C distances average 1.398(21) Å. The longer C−C distances for **1b**$_2$-μ-toluene in comparison to those found in free toluene or toluene radical anion are consistent with a substantial covalent overlap between filled uranium f orbitals and LUMOs of the bridging toluene, as found from DFT calculations on model compounds.[1] Furthermore, high-level CASSCF calculations support this conclusion (see Computational Results).

NMR Spectroscopy Studies on 1a$_2$-μ-toluene: Probing Stability and Fluxionality. ^{1}H NMR analysis showed that the bridging toluene in **1a**$_2$-μ-toluene exchanges slowly with C$_6$D$_6$ (5% exchange in 24 h) at room temperature. Since **1a**$_2$-μ-toluene is thermally stable,[1] arene exchange was also studied at higher temperatures. Preliminary results show that the bridged toluene exchanges with C$_6$D$_6$ faster than the bridged benzene in (μ-benzene)U$_2$(N[^{t}Bu]Ar)$_4$ (**1a**$_2$-μ-benzene)[1] exchanges with toluene-d_8. Furthermore, the bridging toluene did not exchange with *p*-xylene over a 24 h period. These results are similar to those reported by Evans et al.[2] and show an opposite trend from that found for transition-metal complexes.[41] For transition-metal complexes, the bond between the HOMOs of the arene and empty metal d orbitals dictates such behavior; hence, a less electron rich arene, such as benzene, will exchange for a more electron rich substrate, such as toluene or mesitylene. For the uranium complexes, the exchange studies reflect the existence of a back-bond from filled uranium f orbitals to LUMOs of the arene and a less electron rich ligand is preferred to a more electron rich analogue.

1a$_2$-μ-toluene is dinuclear in the solid state. In order to test whether in solution there is an equilibrium between the dinuclear structure and some mononuclear species (either two uranium bis(amide) fragments or a uranium bis(amide) fragment and a coordinated benzene uranium bis(amide) fragment), the variable-temperature (VT) behavior of **1a**$_2$-μ-toluene was examined between −70 and 120 °C (the compound is stable at these temperatures during the time of the experiment). Figure 4 presents the plot of δ versus $1/T$ for all of the protons of the molecule. Although the graphs for the protons belonging to the bridging toluene are slightly curved, those for the amide protons are linear, indicating Curie−Weiss behavior.[42] This finding suggests that the dinuclear compound is the only species in solution detectable by NMR spectroscopy.

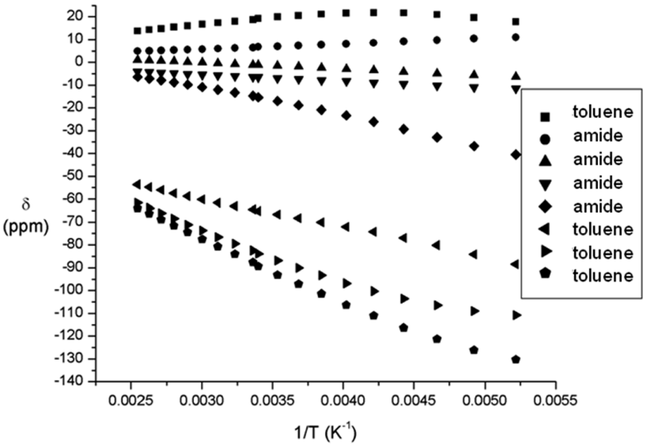

Figure 4. Plot of δ versus $1/T$ for **1a**$_2$-μ-toluene.

Electronic Spectra. Electronic spectra of uranium complexes are usually complicated due to the splitting by ligand-field and spin−orbit coupling of a multitude of states derived from f^n configurations. The electronic spectra are comprised of f → f, f → d, and charge-transfer bands. Usually, bands are assigned on the basis of the magnitude of the molar absorption coefficient and the position of a band in a spectrum.[33,43−45] Therefore, for the compounds discussed here, bands present in the UV region (200−400 nm), due to their high intensity ($\varepsilon \approx 10^5$ M^{-1} cm^{-1}), can be assigned to $\pi \rightarrow \pi^*$ transitions of the arene rings (see the Supporting Information, Figures SX5 and SX6). Additionally, intense absorption bands present in the visible region (400−800 nm) that have $\varepsilon \approx 10^3$ M^{-1} cm^{-1} could be either f → d or charge-transfer transitions (Figures SX5 and SX6).

The most interesting region of the electronic spectra for uranium compounds is the near-IR region (spectra reported here were recorded from 1500 to 800 nm, Figure 5), because most compounds show "fingerprint" features. These characteristics are assigned to Laporte-forbidden f → f transitions and have molar absorption coefficients in the range 10−10^2 M^{-1} cm^{-1}. With the exception of the U(III) compound **2b**-THF (ε = 100−260 M^{-1} cm^{-1}) the other mononuclear compounds

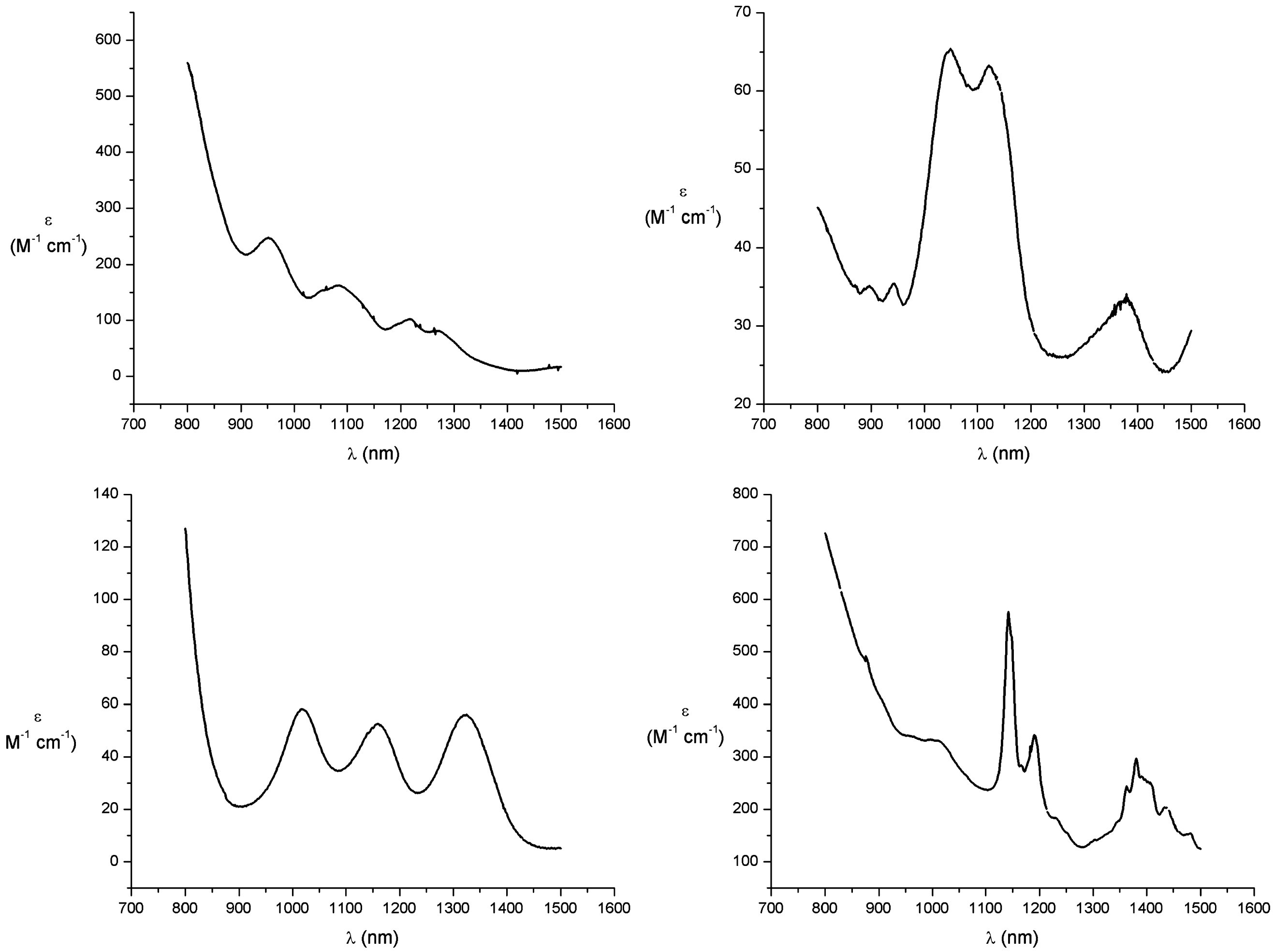

Figure 5. Near-IR spectra at 25 °C of **2b**-THF in THF (top left), **2b**-I in toluene (top right), **2b**-NSiMe$_3$ in toluene (bottom left), and **1a**$_2$-μ-toluene in toluene (bottom right).

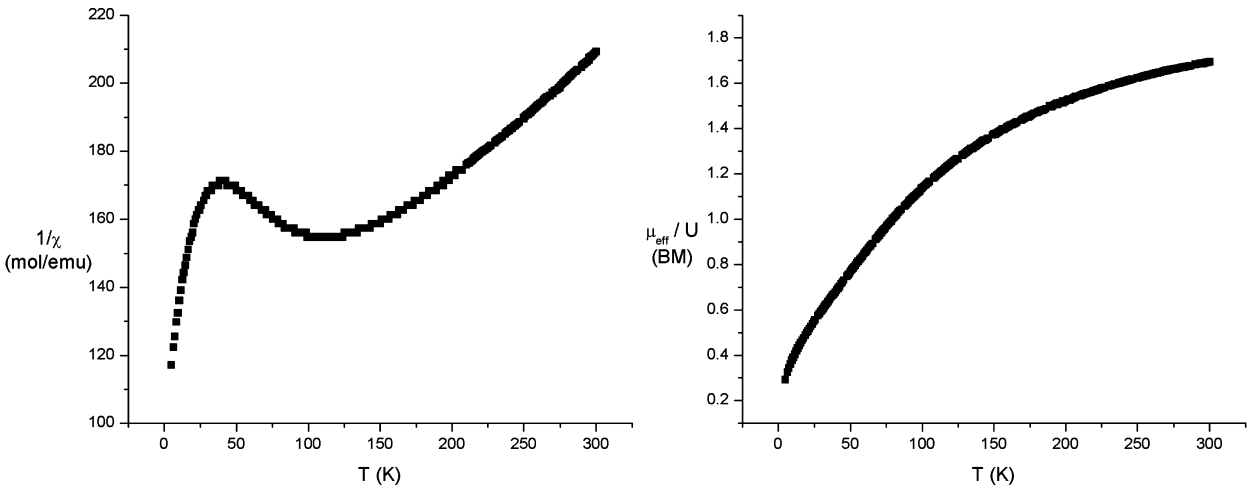

Figure 6. Plots of $1/\chi$ (left) and μ_{eff} (right) versus T for **1a**$_2$-μ-toluene.

show weak bands in the near-IR region ($\varepsilon < 100$ M^{-1} cm^{-1}). As observed for other toluene or benzene-bridged diuranium systems,[2,5] **1a**$_2$-μ-toluene has intense bands ($\varepsilon = 200-600$ M^{-1} cm^{-1}) in this region. The increased intensity of the f−f transitions in uranium complexes has previously been attributed to intensity stealing,[46] which is an increase in intensity in formally forbidden transitions due to the presence of significant covalent bonding.[47] The observation of intense f−f bands for only **1a**$_2$-μ-toluene suggests that the bonding between the uranium centers and the bridging toluene ligand is significantly covalent. Previous reports used the similarity between the near-IR spectra of toluene or benzene-bridged diuranium systems and uranium(III) complexes as an indication that the electronic structure of the diuranium compounds is consistent with the

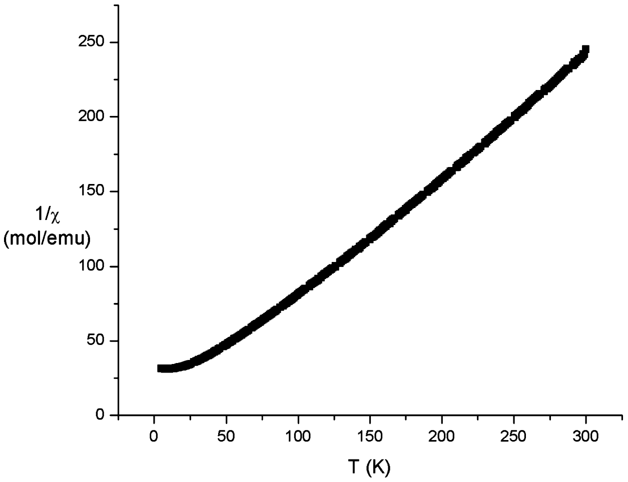

Figure 7. Plots of $1/\chi$ versus T for **2a**-I (left) and **2b**-I (right).

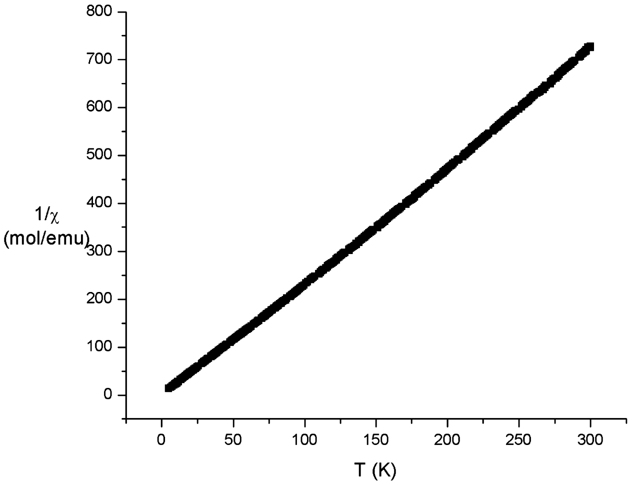

Figure 8. Plots of $1/\chi$ versus T for **2b**-THF (left) and **2b**-$NSiMe_3$ (right).

presence of uranium(III) metal centers, in agreement with our XANES results (see below).

Solid-State Magnetic Susceptibility Measurements. Although magnetic properties of uranium compounds are usually difficult to interpret,[48,49] SQUID measurements were carried out on the whole series of complexes considered here in order to compare the behavior of the mononuclear compounds to that of **1a**$_2$-μ-toluene. It is notable that the magnetic moment for **1a**$_2$-μ-toluene (Figure 6) is temperature dependent (from 0.25 μ_B at 5 K to 1.50 μ_B at 300 K; values for one uranium center), while the mononuclear compounds present Curie–Weiss behavior in the 5–300 K temperature range (except for the TIP intervals for **2a**-I and **2b**-I, Figure 7). In addition, for **1a**$_2$-μ-toluene (Figure 6), although paramagnetic behavior is observed over the temperature intervals 5–50 and 170–300 K, as the temperature is lowered to around 125 K, the magnetic susceptibility of the sample passes through a maximum and begins to decrease at lower temperatures. Between 95 and 125 K the minimum values in the $1/\chi$ versus T graph are characteristic of a transition to antiferromagnetic behavior.[5,50,51]

This overall behavior is in contrast to that found for the analogous bridging-toluene complex $[(U(BIPM^{TMS}H)(I))_2(\mu\text{-}\eta^6{:}\eta^6\text{-}C_6H_5CH_3)]$ ($BIPM^{TMS} = C(PPh_2NSiMe_3)_2$), which did not show strong antiferromagnetic coupling.[5]

The magnetic behavior of the mononuclear complexes is as expected and follows some general trends. For example, at low temperatures, the graphs for **2a**-I and **2b**-I (Figure 7) show temperature-independent paramagnetism (TIP, 5–25 K for **2a**-I and 5–15 K for **2b**-I). TIP behavior is specific to even-electron species, since at low temperatures the ground state can be an orbital singlet.[52] Kramers ions, i.e. odd-electron species, such as the U(III) (**2b**-THF) and U(V) (**2b**-$NSiMe_3$) compounds (Figure 8), would never present a singlet ground state; therefore, their low-temperature magnetic behavior is different from that of U(IV) compounds. The determined μ_{eff} values for **2b**-THF (3.20 μ_B), **2b**-I (3.52 μ_B, 20–300 K), and **2a**-I (3.18 μ_B, 50–300 K) are within the range for uranium(III) and uranium(IV) complexes. The magnetic moment obtained for **2b**-$NSiMe_3$ is 1.81 μ_B, smaller than the other magnetic moments of the mononuclear compounds but consistent with values for similar uranium(V) compounds.[53]

X-ray Absorption Near-Edge Structure (XANES) Spectroscopy Results. The chemical shift of the absorption edge reflects the effective charge of the absorbing atom.[54,55] For uranium complexes, the U L_3 absorption edge, which corresponds to a $2p_{3/2}$ to $6d_{5/2}$ transition, has been shown to vary systematically with the uranium oxidation state.[56,57] Therefore, the chemical shifts of the U L_3 absorption edge are affected by changes in shielding of the $2p_{3/2}$ electrons and can be used to compare the effective charges on the uranium centers in different complexes. Although effective charges can be correlated to the oxidation state of the absorbing atom, other factors, including coordination geometry and the degree of covalency in the ligand−metal interactions, may also be significant. For a series of formally trivalent organometallic and inorganic uranium compounds, the average chemical shift of the absorption edge relative to a UO_2Cl_2 sample is −6.0(5) eV, and for a series of formally tetravalent uranium complexes, the average shift is −3.1(6) eV, as shown in Table 1 and Figure 9. Both sets of compounds include different coordination geometries and ligands with widely varying electronegativities.

Table 1. U L_3 Chemical Shifts of Uranium Complexes[a]

compound	edge shift versus 0.1 M UO_2Cl_2 (eV)	oxidation state
$1a_2$-μ-toluene	−5.1	3
$U[N(SiMe_3)_2]_3$	−6.3	3
$[Cp^{\ddagger}_2UOH]_2$[58]	−6.4	3
$[Cp^{\ddagger}_2UF]_2$[58]	−5.0	3
$[Cp^{\ddagger}_2UCl]_2$[58]	−6.3	3
$[Cp^{\ddagger}_2UBr]_2$[58]	−5.7	3
$[Cp''_2UF]_2$[58]	−5.9	3
$[Cp''_2UCl]_2$[58]	−6.4	3
$[Cp''_2UBr]_2$[58]	−5.6	3
$IU(DME)(NC[^tBu]Mes)_3$[10]	−3.3	4
2a-I	−3.8	4
$[Cp^{\ddagger}_2UO]_2$[58]	−2.0	4
$Cp^{\ddagger}_2UF_2$[58]	−2.4	4
$Cp^{\ddagger}_2UCl_2$[58]	−2.9	4
$Cp^{\ddagger}_2UBr_2$[58]	−3.5	4
$Cp^{\ddagger}_2UI_2$[58]	−3.6	4
Cp''_2UF_2[58]	−2.6	4
Cp''_2UCl_2[58]	−2.4	4
Cp''_2UBr_2[58]	−3.7	4
Cp''_2UI_2[58]	−3.6	4

[a] Abbreviations: $Cp^{\ddagger}$ = 1,3-$(Me_3C)_2C_5H_3$, Cp'' = 1,3-$(Me_3Si)_2C_5H_3$, DME = 1,2-dimethoxyethane.

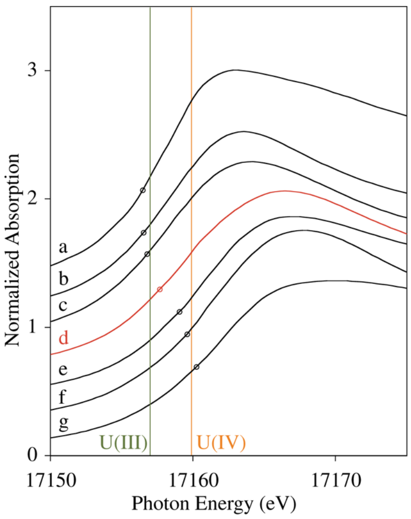

Figure 9. U L_3 absorption edges of selected organouranium complexes. The edge height is normalized such that the absorption at the edge step is equal to 1. The edge energies are referenced to the half-height of a 0.1 M UO_2Cl_2 in 1 M HCl solution set at 17163 eV. The compounds are (a) $U[N(SiMe_3)_2]_3$, (b) $[Cp''_2UCl]_2$,[58] (c) $[Cp^{\ddagger}_2UOH]_2$,[58] (d) $(\mu$-$C_7H_8)[U(N[^tBu]Ar)_2]_2$ (**$1a_2$**-μ-toluene), (e) $IU(N[^tBu]Ar)_3$ (**2a**-I), (f) $IU(DME)(NC[^tBu]Mes)_3$,[10] and (g) $(Me_3SiN)U(N[Ad]Ar)_3$ (**2b**-$NSiMe_3$). The point closest to the half-height is circled. The average edge shifts of U(III) and U(IV) complexes are indicated by the vertical lines.

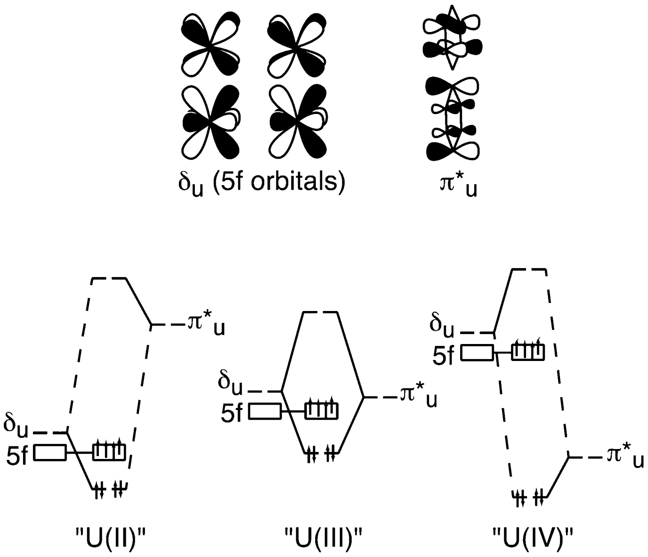

Figure 10. Bonding scenarios in arene-bridged diuranium complexes. The relative energies of the 5f and π_u orbitals affect the XANES edge shift.

In the family of complexes $(\mu$-arene$)[U(N[R]Ar)_2]_2$, the bonding lies somewhere between two extremes: (1) a neutral arene ligand coordinated by two U(II) centers and (2) an arene tetraanion with two U(IV) centers (Figure 10). A series of the U L_3 absorption edges of selected uranium complexes is shown in Figure 9. Since the chemical shift of **$1a_2$**-μ-toluene is −5.1 eV, the effective charge of the U center in the complex is mostly similar to that of U(III) complexes. A description of the bonding more detailed than that presented here requires information about the overlap between the ligand and metal orbitals,[59] as well as their relative energies. Nonetheless, the observed chemical shift of the U L_3 edge is consistent with a strong, covalent interaction between the arene π_u* orbitals and the δ_u orbitals of the two uranium centers. In particular, the observed chemical shift of **$1a_2$**-μ-toluene is consistent with its formulation as two U(III) centers bridged by a toluene(2−) ligand, where the f electrons on the U(III) center are stabilized by back-bonding with the bridging ligand.

It is important to note that the bonding picture described here shares characteristics with those of actinocene complexes $An(C_8H_8)_2$ (An = actinide), which have been intensely researched and investigated.[60−62] The similarities between the two classes of complexes stem from the analogous symmetry of frontier orbitals for both the metal and the arene ligand. The differences consist of the oxidation state of the metal and the energy of arene orbitals. As pointed out recently,[63] tuning of both contributors influences greatly the extent of covalency in actinide complexes.

Computational Results. *DFT Calculations.* Geometries were optimized for the DFT ground state for model systems based on the **2b**-THF, **2b**-I, **2b**-$NSiMe_3$, and **$1a_2$**-μ-toluene structures. **2b**-THF and **2b**-I are U(III) and U(IV) compounds and have quartet and triplet ground states, respectively. In both cases, the experimental and calculated structures are in very

Table 2. Average Distances (Å) and Angles (deg) for Calculated and Experimentally Obtained Structures

		av distance (Å)		angle (deg)	
		U–N	U–X	X–U–N	U–Y–Z
2b-THF (X = O)	exptl	2.35	2.49	98.89/108.2/116.0	
	B-97D	2.30	2.50	92.3/115.6/116.3	
	PBE	2.32	2.41	96.0/107.8/121.9	
2b-I (X = I)	exptl	2.20	3.07	94.3/113.3/126.2	
	B-97D	2.23	3.07	92.2/113.0/123.2	
	PBE	2.23	3.07	91.7/113.9/125. 8	
2b-$NSiMe_3$ (X, Y = N_{imide}; Z = Si)	exptl	2.25	1.94	103.2/103.7	170.3
	B-97D	2.27	1.94	102.4/103.2	168.8
	PBE	2.28	1.95	106.0/108.6	171.2
1a$_2$-μ-toluene (X = N; Y = U; Z = N)	exptl	2.33	2.59	103.2/103.7	126.4/127.0/129.8/129.9
	B-97D	2.33	2.62	104.2/105.3	124.7/126.2/128.2/130.6
	PBE	2.33	2.60	103.8/104.6	126.4/127.0/128.3/129.5

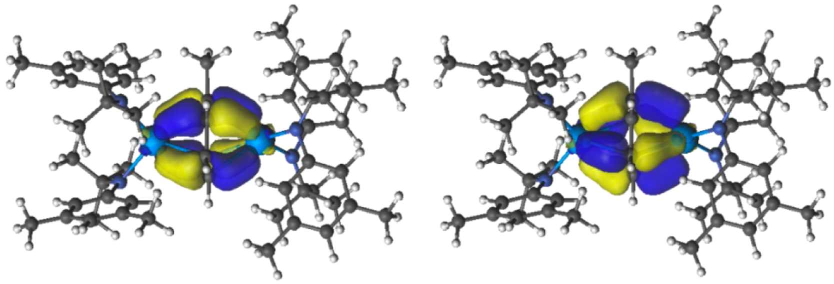

Figure 11. δ bonding natural orbitals[66] from **1a**$_2$-μ-toluene. From left to right, the natural orbital occupation numbers are 1.86 and 1.87. Legend: U, light blue; N, blue; C, gray; H, white.

good agreement, as shown in Table 2 and Table S1 (Supporting Information). Both doublet and quartet spin states were explored for **2b**-$NSiMe_3$. The doublet is 33.3 kcal/mol lower in energy at the B-97D level of theory than for the quartet. Moreover, the doublet geometry is in good agreement with experimental parameters, whereas the quartet has an average U–N_{amide} distance of 2.40 Å, as opposed to the 2.24 Å observed experimentally. Finally, **1a**$_2$-μ-toluene was optimized for the quintet state. While the singlet and triplet spin states should be considered, these states suffer from spin contamination at the DFT level, and therefore the energetics are unreliable. For this reason, only the quintet state was considered with DFT, while all of the spin states were studied at the CASSCF/CASPT2 level of theory (see below). Average distances and angles are in good agreement with experimental parameters (Table 2). The dihedral angles are expected to deviate more than the other parameters due to the ligand truncation; however, the calculated values are within 10° of experiment (Table S1), with the exception of the B-97D N_{imide}–U–N–$C_{tert\text{-}butyl}$ dihedral angle in **2b**-$NSiMe_3$, which deviates by 15°.

CASSCF/CASPT2 Results. The electronic structure was further explored by performing complete active space self-consistent field calculations with corrections from second-order perturbation theory (CASSCF/CASPT2) on the optimized geometries. In CASSCF, a set of orbitals in the valence region is defined, together with the electrons associated with these orbitals. Within this orbital space, which is referred to as the active space, the electronic configurations that can be obtained by distributing the electrons in the active orbitals in all possible ways are considered.[64] The total wave function is constructed as a linear combination of all these electronic configurations. The orbitals lower in energy than the active space are doubly occupied, while those that are higher in energy are unoccupied. When possible, all valence orbitals should be included in the active space; however, in practice this is not always required. For the higher oxidation states of uranium, it is common practice to include only the seven U 5f orbitals in the active space, since the 6d and 7s orbitals are higher in energy and consequently unoccupied.[65] For **2b**-THF and **2b**-I, the ligands do not engage in strongly covalent interactions with the U center, and as a result only the 5f orbitals need to be included in the active space with either three or two electrons, respectively (see Figures S8 and S9 in the Supporting Information). The ground state of **2b**-THF is a quartet, while the ground state of **2b**-I is a triplet, as expected for U(III) and U(IV) compounds, respectively.

Alternatively for **2b**-$NSiMe_3$, including only the seven U 5f orbitals in the active space would not properly describe the covalent bonding between the imide nitrogen and uranium. For this reason, the three N 2p orbitals must be included in the active space as well, resulting in an active space of 7 electrons in 10 orbitals. However, in practice this space was too small, as CASSCF and CASPT2 predicted different ground states. We found that including 6 additional doubly occupied orbitals containing contributions from the U 6p, U 5d, and N 2s orbitals in the active space was very important in obtaining consistency between CASSCF and CASPT2 energies. With this larger space of 19 electrons in 15 orbitals, the doublet was the ground state at the CASSCF and CASPT2 levels by 51.5 and 18.7 kcal mol^{-1}, respectively. Furthermore, the bond between U and N_{imide} is a double bond, as shown in Figure S10 (Supporting Information).

For **1a**$_2$-μ-toluene, the active space consists of 8 electrons in 14 orbitals. One can think of this as including the 7 U 5f orbitals on each center and the corresponding electrons;

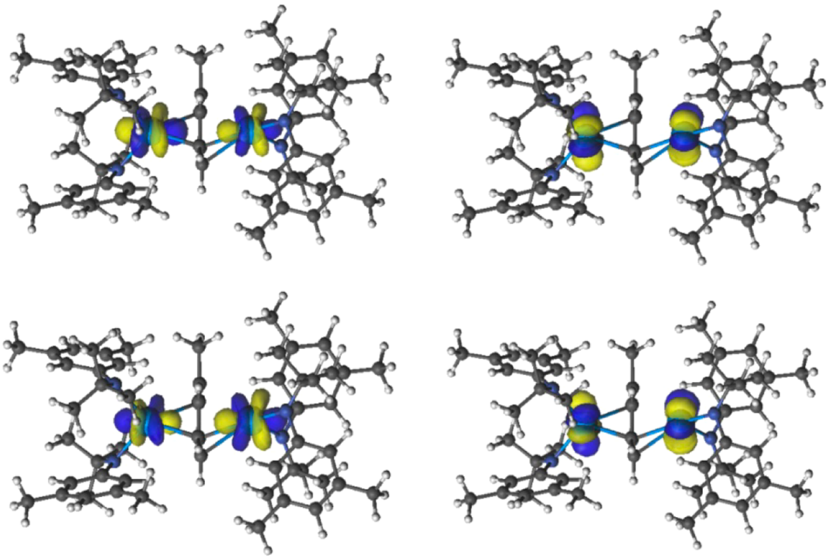

Figure 12. Singly occupied natural orbitals of **1a**$_2$-μ-toluene. Legend: U, light blue; N, blue; C, gray; H, white.

however, the resulting molecular orbitals corresponding to U−arene−U bonding contain contributions from both 5f and 6d orbitals. The singlet, triplet, quintet, and septet spin states were explored. The ground state at the CASPT2 level is the singlet; however, the triplet and quintet are only 0.7 and 2.5 kcal mol^{-1} higher in energy, respectively. Spin−orbit effects were not included in these calculations. Additionally, the orbital pictures are the same for all three states. Two sets of δ bonds composed of occupied uranium 5f orbitals donating into π antibonding orbitals on the toluene group are present along with four singly occupied 5f orbitals (Figures 11 and 12). The quintet is high spin and consists of one dominating configuration contributing 87% to the total wave function. Alternatively, the singlet and triplet are much more multireference in nature and the total wave function contains contributions from several electronic configurations (Table 3). Finally, the septet state was explored and is 34.5 kcal mol^{-1} higher in energy than the singlet.

Table 3. Electronic Configurations Contributing to the Total Wave Function in 1a$_2$-μ-toluene

spin state	configuration	% of the total wave function
quintet	$\delta^2\delta^2 5f^1 5f^1 5f^1 5f^1$	87.1
triplet	$\delta^2\delta^2 5f^1 5f^2 5f^1 5f^0$	17.1
	$\delta^2\delta^2 5f^2 5f^1 5f^0 5f^1$	21.2
	$\delta^2\delta^2 5f^0 5f^1 5f^2 5f^1$	20.6
	$\delta^2\delta^2 5f^1 5f^0 5f^1 5f^2$	17.4
singlet	$\delta^2\delta^2 5f^2 5f^2 5f^0 5f^0$	14.2
	$\delta^2\delta^2 5f^2 5f^0 5f^2 5f^0$	13.9
	$\delta^2\delta^2 5f^1 5f^1 5f^1 5f^1$	14.3
	$\delta^2\delta^2 5f^0 5f^2 5f^0 5f^2$	13.7
	$\delta^2\delta^2 5f^0 5f^0 5f^2 5f^2$	13.5

Table 4. LoProp Charges for the Ground State CASSCF Wave Function

	2b-THF	**2b**-I	**2b**-NSiMe$_3$	**1a**$_2$-μ-toluene
U	2.20	2.76	3.04	2.33/2.34
N	−0.84	−0.84	−0.79	−0.54
	−0.77	−0.86	−0.85	−0.52
	−0.80	−0.85	−0.83	−0.54
				−0.54
other	−0.55 (O)	−0.75 (I)	−1.29 (N$_{\text{imide}}$)	−1.95 (toluene (sum))

LoProp Charges. Atomic charges were computed from the CASSCF results using the LoProp approach (Table 4). LoProp charges are reported, since this procedure is stable with respect to the basis set and provides physically meaningful localized properties.[67] First, by comparison of the uranium partial charges it is observed that, as expected, the partial charge of the U(III) compound **2b**-THF is less than that of the U(IV) compound **2b**-I. Additionally, the ground state of **2b**-NSiMe$_3$ is a doublet, corresponding to a U(V) center. The partial charge on uranium in **2b**-NSiMe$_3$ is consistent with this assignment, as it is higher than in **2b**-I. Finally, the partial charges on the U centers in **1a**$_2$-μ-toluene are consistent with a +3 oxidation state. Additionally, the sum of the charges on the bridging toluene group is −1.95, indicating that charge transfer occurs from the uranium centers to the bridging toluene ligand, which is consistent with both the observed reactivity (**1a**$_2$ coordinated preferentially the least electron rich bridging arene) and the chemical shift observed by XANES spectroscopy.

Consistent with a +5 oxidation state assignment, the reaction of **2b**-NSiMe$_3$ with lithium under argon or with KC$_8$ in THF resulted in the formation of [Li(OEt$_2$)][(Me$_3$SiN)U(N[Ad]Ar)$_3$] (Li[**2b**-NSiMe$_3$]; Figure 13) or K[(Me$_3$SiN)U(N[Ad]Ar)$_3$] (K[**2b**-NSiMe$_3$]; eq 2). The longer distances U−N$_{\text{amide}}$ = 2.357(5) Å (av) and U−N$_{\text{SiMe}_3}$ = 2.050(3) Å as compared to the corresponding values in **2b**-NSiMe$_3$ are indicative of a more electron rich uranium center.

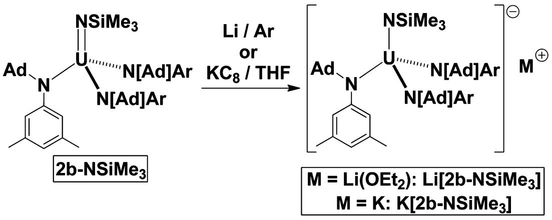

(2)

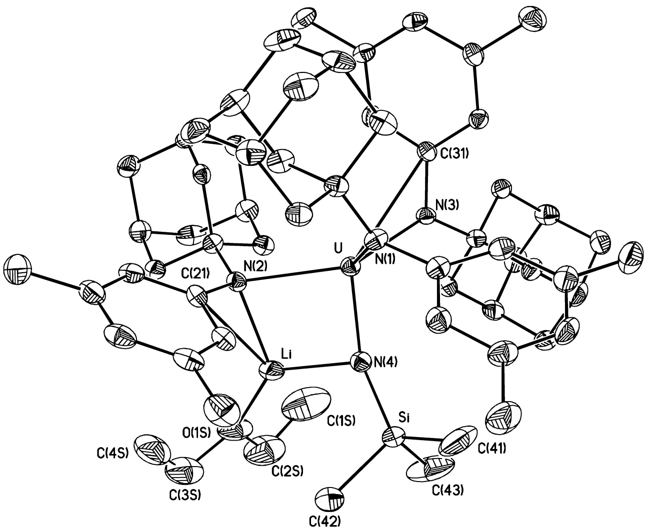

Figure 13. Structural drawing of [Li(OEt$_2$)][(Me$_3$SiN)U(N[Ad]Ar)$_3$] (Li[**2b**-NSiMe$_3$]) with thermal ellipsoids at the 35% probability level and hydrogen atoms omitted for clarity. Selected distances (Å): U−N$_{\text{ligand}}$(av), 2.357(5); U−N$_{\text{imide}}$, 2.050(3).

■ CONCLUSIONS

The compound **1a**$_2$-μ-toluene was studied in relation to a variety of mononuclear uranium amide complexes, and its properties were discussed with reference to their properties. While the mononuclear compounds display the expected electronic and magnetic properties, **1a**$_2$-μ-toluene showed complicated characteristics in contrast. The optical and magnetic properties of **1a**$_2$-μ-toluene are difficult to relate to reported examples of mononuclear uranium organometallic complexes. XANES spectroscopy, X-ray crystallography, and computational studies corroborate the following electronic structure interpretation: the f orbitals of the two uranium centers host the four unpaired electrons, followed energetically by two covalent δ bonds formed by filled uranium f orbitals overlapping with the LUMOs of toluene, in accord with our original analysis.[1] An effective electronic charge of the metal centers was determined by XANES and is comparable to values encountered for classical uranium(III) compounds; these results are consistent with the presence of a covalent bond between uranium and toluene that is reflected in the metrical parameters of **1b**$_2$-μ-toluene, as determined by X-ray crystallography.

■ EXPERIMENTAL SECTION

General Considerations. Unless stated otherwise, all operations were performed in a Vacuum Atmospheres drybox under purified nitrogen or using Schlenk techniques under an argon atmosphere. Anhydrous diethyl ether was purchased from Mallinckrodt; *n*-pentane, *n*-hexane, and tetrahydrofuran (THF) were purchased from EM Science. Diethyl ether, toluene, benzene, *n*-pentane, and *n*-hexane were dried and deoxygenated by the method of Grubbs.[68] THF was distilled under nitrogen from purple sodium benzophenone ketyl and was transferred under nitrogen into glass vessels before being pumped into the drybox. C$_6$D$_6$ was purchased from Cambridge Isotopes and was degassed and dried over 4 Å sieves. The 4 Å sieves, alumina, and Celite were dried under reduced pressure overnight at a temperature just above 200 °C. UI$_3$(THF)$_4$,[33] KC$_8$,[69] KCH$_2$C$_6$H$_5$,[70] HN[Ad]Ar,[71] and compounds **1a**$_2$-μ-toluene,[1] **1b**$_2$-μ-toluene,[1] **2a**-I,[1] **2b**-I[21] were prepared according to literature methods. Me$_3$SiN$_3$ was passed through alumina and stored in a refrigerator at −35 °C. Other chemicals were used as received. ^{1}H NMR spectra were recorded on Varian XL-300 and Varian INOVA-501 spectrometers at room temperature unless specified otherwise. Chemical shifts are reported with respect to internal or external solvent: 7.16 ppm (C$_6$D$_6$). UV−vis spectra were recorded on a HP spectrophotometer from 200 to 1100 nm using matched 1 cm quartz cells, and near-IR spectra were recorded on a PS spectrophotometer from 800 to 1500 nm using matched 1 cm quartz cells; all spectra were obtained using a solvent reference blank. Numerical modeling of all data was done using the program Origin 6.0. CHN analyses were performed by H. Kolbe Mikroanalytisches Laboratorium (Mülheim an der Ruhr, Germany).

Synthesis of KN[Ad]Ar. A 500 mL round-bottom flask was charged with HN[Ad]Ar (8.52 g, 33 mmol) and diethyl ether (300 mL), and the solution was frozen. Solid KCH$_2$C$_6$H$_5$ (4.35 g, 33 mmol) was added to the thawing solution, and the reaction mixture was warmed to room temperature and stirred for 2−3 h. Filtration of the resulting solution afforded a white solid that was washed with pentane and dried under reduced pressure. The KN[Ad]Ar obtained amounted to 7.93 g (27 mmol, 82% yield). ^{1}H NMR (300 MHz, C$_6$D$_6$, 22 °C): δ 6.28 (s, 1H, *p*-Ar); 6.22 (s, 2H, *o*-Ar); 2.23 (s, 6H, Ar-*Me*); 1.95 (s, 3H, Ad-C*H*); 1.83 (s, 6H, Ad-C*H*$_2$); 1.52 (s, 6H, Ad-C*H*$_2$).

Synthesis of (THF)U(N[Ad]Ar)$_3$ (2b-THF). A 100 mL round-bottom flask was charged with UI$_3$(THF)$_4$ (0.526 g, 0.56 mmol), KN[Ad]Ar (0.510 g, 1.74 mmol, 3 equiv), and a stirring bar and then placed in the cold well. Thawing THF (50 mL) was added to the solid mixture as quickly as possible and the reaction mixture stirred for 45 min. Filtration of the reaction mixture through Celite afforded a solution from which the solvent was removed. The solid obtained was collected on a frit and washed with small portions of diethyl ether (2 × 15 mL). The solid obtained on the frit was dried and redissolved in diethyl ether, and the solution was concentrated and placed in a freezer at −35 °C. After several days, the solution was decanted and the black microcrystalline solid (**2b**-THF; 0.304 g, 0.29 mmol, 51% yield) dried under reduced pressure. ^{1}H NMR (300 MHz, C$_6$D$_6$, 22 °C): δ 37.55 (s, 4H, THF-C*H*$_2$); 0.65 (bs, 9H, *o*- and *p*-Ar); 0.23 (s, 9H, Ad-C*H*); 0.13 (d, 18H, Ad-C*H*$_2$); −0.13 (d, 18H, Ad-C*H*$_2$); −6.64 (s, 18H, Ar-*Me*); −15.80 (s, 4H, THF-C*H*$_2$). Anal. Calcd for C$_{58}$H$_{83}$N$_3$OU: C, 64.72; H, 7.77; N, 3.90. Found: C, 64.79; H, 7.93; N, 3.72.

Synthesis of (Me$_3$SiN)U(N[Ad]Ar)$_3$ (2b-NSiMe$_3$). *(a). From* ***2b*****-*****THF*****.** Solutions in THF of **2b**-THF (1.169 g, 1.14 mmol, 80 mL) and Me$_3$SiN$_3$ (0.144 g, 1.25 mmol, 1.1 equiv, 20 mL) were frozen. To the thawing solution of **2b**-THF was added dropwise a solution of Me$_3$SiN$_3$, and the reaction mixture was warmed to room temperature and stirred for 1 h. After the reaction was finished, the solvent was removed under reduced pressure, the obtained solid was dissolved in pentane, and the new solution was concentrated and stored at −35 °C for several days. **2b**-NSiMe$_3$ was obtained as a black, crystalline solid in two crops amounting to 0.586 g (0.56 mmol, 49% yield).

(b). From UI$_3$(THF)$_4$ Directly. UI$_3$(THF)$_4$ (1.193 g, 1.31 mmol) and KN[Ad]Ar (1.156 g, 3.94 mmol, 3 equiv) were mixed as solids in a 250 mL round-bottom flask and placed in the cold well. To the stirred mixture was added thawing THF (100 mL). The reaction mixture was warmed to room temperature and stirred for a total of 35 min, after which it was filtered through Celite and and the resulting solution frozen again. To this thawing solution was added dropwise a thawing solution of Me$_3$SiN$_3$ (0.136 g, 1.18 mmol, 0.9 equiv) in THF (20 mL). After the addition was finished, the removal of solvent was started immediately. The obtained solid was extracted with pentane, and the solution was filtered through Celite. The solvent was removed, and the last two operations were repeated. The new solution was concentrated to ca. 20 mL and placed in a −35 °C freezer. **2b**-NSiMe$_3$ was obtained as a black, crystalline solid in two crops amounting to 0.521 g (0.50 mmol, 38% yield). ^{1}H NMR (300 MHz, C$_6$D$_6$, 22 °C): δ 11.95 (bs, 2H, *o*-Ar); 8.28 (s, 3H, Si-C*H*$_3$); 6.24 (s, 1H, *p*-Ar); 2.03 (s, 6H, Ar-*Me*); 1.09 (s, 3H, Ad-C*H*); −0.06 (d of d, 6H, Ad-C*H*$_2$); −5.59 (bs, 6H, Ad-C*H*$_2$). Anal. Calcd for C$_{57}$H$_{81}$N$_4$SiU: C, 62.90; H, 7.50; N, 5.15. Found: C, 62.80; H, 7.52; N, 5.11.

Synthesis of [Li(OEt$_2$)][(Me$_3$SiN)U(N[Ad]Ar)$_3$]. Small cubes of lithium (two to three) were washed with hexanes and transferred under argon to a round-bottom flask charged with a magnetic stirring bar. To this flask was transferred via cannula a THF solution (25 mL) of **2b**-$NSiMe_3$ (0.699 g, 0.67 mmol) prepared in the glovebox. The reaction mixture was stirred for 2 h at room temperature, after which the solvent was removed under reduced pressure. The flask was taken into the box, the solid obtained was extracted with pentane, and the new solution was filtered through Celite. After the solvent was removed from the filtrate, extraction with pentane and filtration were repeated and the new solution was concentrated and placed in a −35 °C freezer. $[Li(OEt_2)][(Me_3SiN)U(N[Ad]Ar)_3]$ was obtained as orange crystals in two crops amounting to 0.502 g (0.43 mmol, 64% yield). ^1H NMR (300 MHz, C_6D_6, 22 °C): δ 11.49 (bs, 6H, Et_2O-CH_3); 10.61 (bs, 6H, *o*-Ar); 9.12 (s, 9H, Si-CH_3); 8.10 (s, 3H, *o*-Ar); 7.13 (d, 4H, Et_2O-CH_2); 2.06 (s, 18H, Ar-*Me*); −1.99 (d of d, 18H, Ad-CH_2); −3.34 (s, 9H, Ad-*CH*); −15.16 (bs, 18H, Ad-CH_2). Anal. Calcd for $C_{61}H_{91}N_4SiOLiU$: C, 62.59; H, 7.78; N, 4.79. Found: C, 62.60; H, 8.35; N, 4.71.

Synthesis of $K[(Me_3SiN)U(N[Ad]Ar)_3]$. A thawing slurry of KC_8 (0.188 g, 1.39 mmol, 2.8 equiv) in THF (15 mL) was added dropwise to a thawing THF solution (20 mL) of **2b**-$NSiMe_3$ (0.518 g, 0.50 mmol). The reaction mixture was warmed to room temperature and stirred for 1.5 h, after which the solvent was removed under reduced pressure. The solid obtained was extracted with diethyl ether and the new solution filtered through Celite. After the solvent was removed from the filtrate, the extraction with diethyl ether and the filtration were repeated and the new solution was concentrated and placed in a −35 °C freezer. K[**2b**-$NSiMe_3$] was obtained as dark orange crystals in one crop amounting to 0.415 g (0.38 mmol, 77% yield). ^1H NMR (300 MHz, C_6D_6, 22 °C): δ 20.67 (s, 3H, Si-CH_3); 4.75 (s, 1H, *p*-Ar); 1.99 (s, 3H, Ad-*CH*); 0.82 (d of d, 6H, Ad-CH_2); 0.09 (s, 6H, Ar-*Me*); −1.05 (bs, 2H, *o*-Ar); −2.58 (bs, 6H, Ad-CH_2).

Thermal Stability of $1a_2$-μ-toluene. In one experiment, variable-temperature ^1H NMR studies in octane-d_{18} showed that **$1a_2$**-μ-toluene is stable up to 110 °C. The spectra were acquired from 20 to 110 °C at 10 °C intervals, and after reaching 110 °C, another spectrum was obtained on the same sample back to 20 °C. In another experiment, 40 mg of **$1a_2$**-μ-toluene in 20 mL of heptane was heated at 80 °C for 24 h. A ^1H NMR spectrum of a sample taken from that solution indicated that the compound did not decompose.

Arene Exchange Experiments. **$1a_2$**-μ-toluene was dissolved in C_6D_6, the solution was transferred to an NMR tube, and the NMR tube was sealed and then placed in a heated oil bath. After 24 h at 90 °C, analysis of the ^1H NMR spectrum indicated 3% exchange based on the integration of the peaks at ca. −7 ppm (*Me*-Ar). Integration of the same peak indicated 14% exchange after an additional 24 h at 100 °C and 18% exchange after another 48 h. A similar experiment conducted with **$1a_2$**-μ-benzene dissolved in toluene-d_8 showed 6% exchange after 48 h at 100 °C and 11% exchange on the basis of the integration of the *t-Bu* peaks (ca. 7 ppm) after a total of 96 h. For the exchange experiment with *p*-xylene, **$1a_2$**-μ-toluene was dissolved in *p*-xylene, the solution was transferred to a tube, and the tube was sealed and heated in an oil bath at 90 °C. After 24 h, the tube was taken into the box and broken and its contents were transferred to a vial. Volatiles were removed. Analysis of the compound's ^1H NMR spectrum (C_6D_6, 300 MHz, 22 °C) indicated no transformation of **$1a_2$**-μ-toluene.

X-ray Crystal Structures. X-ray data collections were carried out on a Siemens Platform three-circle diffractometer with a CCD detector using Mo Kα radiation (λ = 0.71073 Å). The data were processed utilizing the program SAINT supplied by Siemens Industrial Automation, Inc. The structures were solved by direct methods (SHELXTL v5.03 by G. M. Sheldrick and Siemens Industrial Automation, Inc., 1995) in conjunction with standard difference Fourier techniques.[72]

XANES Measurements. In an Ar-filled glovebox, approximately 10 mg of uranium complex was powdered and mixed with dry boron nitride. The samples were packaged in aluminum holders with Kapton tape. The samples were sealed in glass jars with Teflon tape inside the drybox. Everything except for the Teflon tape was baked out at 110 °C for several days. The samples showed no signs of decomposition either before or immediately after the XANES experiment. After several hours in the air, the samples began to discolor around the edges. X-ray absorption spectra were acquired at the Stanford Synchrotron Radiation Lightsource (SSRL) at beamline 11-2 or 4-1 using a Si(220) double-crystal monochromator detuned 50% to reduce the higher order harmonic content of the beam. X-ray absorption spectra were obtained in the transmission mode at room temperature using argon-filled ionization chambers. The data analysis was performed by standard procedures using the EXAFSPAK suite of programs developed by G. George of the SSRL. The background was removed by fitting a polynomial to the pre-edge data. Edge shifts are determined from the half-height of the U L_3 absorption edge at 17166 eV and are referenced to the half-height of a 0.1 M solution of UO_2Cl_2 in hydrochloric acid.

Magnetic Susceptibility Measurements. Magnetic susceptibility measurements were recorded using a SQUID magnetometer at 5000 G. The samples were prepared in the glovebox (50−100 mg), loaded in a gelatin capsule that was positioned inside a plastic straw, and carried to the magnetometer in a tube under N_2. The sample was quickly inserted into the instrument and centered, and data were obtained from 5 to 300 K. The contribution from the sample holders was not accounted for. The diamagnetic contributions were calculated and subtracted from χ_{mol}. Effective magnetic moments were calculated either by linear regression from plots of $1/\chi_{mol}$ versus T (K) for Curie−Weiss behavior or by using the formula $2.828(T\chi_{mol})^{1/2}$ for non-Curie−Weiss behavior. Samples used were recrystallized multiple times. Measurements for the same compound were carried out on differently recrystallized samples.

Computational Details. Geometry optimizations were performed with DFT using the Perdew−Burke−Ernzerhof (PBE)[73] exchange-correlation functional and the dispersion corrected B-97D functional[74] with def-TZVP basis sets[75] for all atoms as implemented in the TURBOMOLE 5.10.2 package.[76] The corresponding def-ECP[77] was used for U, and the resolution of the identity (RI) approximation was used for the Coulomb integrals.[64,78] All stationary points were confirmed as minima by vibrational analysis. Due to the large size of the ligands, the 1-adamantyl groups were replaced with *tert*-butyl groups and the 3,5-$C_6H_3Me_2$ groups were replaced with phenyl groups.

Subsequently, the electronic structure was further investigated using complete active space self-consistent field theory (CASSCF)[79] with second-order perturbation theory (CASPT2)[80,81] on top of the B97-D geometry using the Molcas 7.7 package.[82] Relativistic effects were included through the use of the scalar Douglas−Kroll−Hess (DKH) Hamiltonian.[83,84] ANO-RCC basis sets of triple-ζ quality were used for U, O, and N, while a minimal basis set was used for peripheral C and H atoms. In **$1a_2$**-μ-toluene, the C and H atoms of toluene were treated with the ANO-RCC basis set of double-ζ quality.[85,86] Additionally, the Cholesky decomposition technique was used combined with local exchange screening to reduce the computational costs involved in generating the two-electron integrals significantly.[87−90] Atomic charges were computed at the CASSCF level for the ground state using the LoProp procedure.[67]

■ ASSOCIATED CONTENT

Ⓢ Supporting Information

Text, tables, figures, and files giving details of the X-ray crystallographic study, NMR and absorption spectra, coordinates of DFT optimized geometries, and CASSCF orbitals. This material is available free of charge via the Internet at http://pubs.acs.org.

■ AUTHOR INFORMATION

Corresponding Author

*E-mail: pld@chem.ucla.edu (P.L.D.); wwlukens@lbl.gov, (W.L.L.); gagliard@umn.edu (L.G.); ccummins@mit.edu (C.C.C.).

Notes

The authors declare no competing financial interest.

■ ACKNOWLEDGMENTS

For support of this work, we are grateful to the National Science Foundation (CHE-9988806), the Packard Foundation (Fellowship to C.C.C., 1995-2000), and the National Science Board (Alan T. Waterman award to C.C.C., 1998). P.L.D. thanks Daniel J. Mindiola for help with the structures of **2b**-I and **2b**-THF, Dr. Daniel Grohol and Professor Daniel G. Nocera for suggestions and discussions of the magnetic properties, and Aetna Wun for help with recording the near-IR spectra. Portions of this work were supported by the U.S. Department of Energy, Basic Energy Sciences, Chemical Sciences, Biosciences, and Geosciences Division, and were performed at Lawrence Berkeley National Laboratory under Contract No. DE-AC02-05CH11231 and at the Stanford Synchrotron Radiation Lightsource, a Directorate of the SLAC National Accelerator Laboratory and an Office of Science User Facility operated for the U.S. Department of Energy Office of Science by Stanford University. Computational studies were funded by the DOE through Grant No. DE-SC002183.

■ REFERENCES

(1) Diaconescu, P. L.; Arnold, P. L.; Baker, T. A.; Mindiola, D. J.; Cummins, C. C. *J. Am. Chem. Soc.* **2000**, *122*, 6108.
(2) Evans, W. J.; Kozimor, S. A.; Ziller, J. W.; Kaltsoyannis, N. *J. Am. Chem. Soc.* **2004**, *126*, 14533.
(3) Evans, W. J.; Traina, C. A.; Ziller, J. W. *J. Am. Chem. Soc.* **2009**, *131*, 17473.
(4) Evans, W. J.; Kozimor, S. A. *Coord. Chem. Rev.* **2006**, *250*, 911.
(5) Mills, D. P.; Moro, F.; McMaster, J.; van Slageren, J.; Lewis, W.; Blake, A. J.; Liddle, S. T. *Nat. Chem.* **2011**, *3*, 454.
(6) Monreal, M. J.; Khan, S. I.; Kiplinger, J. L.; Diaconescu, P. L. *Chem. Commun.* **2011**, *47*, 9119.
(7) Patel, D.; Moro, F.; McMaster, J.; Lewis, W.; Blake, A. J.; Liddle, S. T. *Angew. Chem., Int. Ed.* **2011**, *50*, 10388.
(8) Arnold, P. L.; Mansell, S. M.; Maron, L.; McKay, D. *Nat. Chem.* **2012**, *4*, 668.
(9) Mougel, V.; Camp, C.; Pécaut, J.; Copéret, C.; Maron, L.; Kefalidis, C. E.; Mazzanti, M. *Angew. Chem., Int. Ed.* **2012**, *124*, 12446.
(10) Diaconescu, P. L.; Cummins, C. C. *J. Am. Chem. Soc.* **2002**, *124*, 7660.
(11) Diaconescu, P. L.; Cummins, C. C. *Inorg. Chem.* **2012**, *51*, 2902.
(12) Arliguie, T.; Lance, M.; Nierlich, M.; Vigner, J.; Ephritikhine, M. *J. Chem. Soc., Chem. Commun.* **1994**, 847.
(13) Arliguie, T.; Lance, M.; Nierlich, M.; Ephritikhine, M. *J. Chem. Soc., Dalton Trans.* **1997**, *14*, 2501.
(14) Lein, M.; Frunzke, J.; Frenking, G. *Inorg. Chem.* **2003**, *42*, 2504.
(15) Kempe, R. *Angew. Chem., Int. Ed.* **2000**, *39*, 468.
(16) Gade, L. H.; Mountford, P. *Coord. Chem. Rev.* **2001**, *216–217*, 65.
(17) Gade, L. H. *J. Organomet. Chem.* **2002**, *661*, 85.
(18) Diaconescu, P. L.; Odom, A. L.; Agapie, T.; Cummins, C. C. *Organometallics* **2001**, *20*, 4993.
(19) Stewart, J. L.; Andersen, R. A. *Polyhedron* **1998**, *17*, 953.
(20) Roussel, P.; Alcock, N. W.; Scott, P. *Chem. Commun.* **1998**, 801.
(21) Odom, A. L.; Arnold, P. L.; Cummins, C. C. *J. Am. Chem. Soc.* **1998**, *120*, 5836.
(22) Arnold, P. L. *Chem. Commun.* **2011**, *47*, 9005.
(23) Diaconescu, P. L. *Acc. Chem. Res.* **2010**, *43*, 1352.
(24) Fox, A. R.; Cummins, C. C. *J. Am. Chem. Soc.* **2009**, *131*, 5716.
(25) Fox, A. R.; Arnold, P. L.; Cummins, C. C. *J. Am. Chem. Soc.* **2010**, *132*, 3250.
(26) Cruz, C. A.; Emslie, D. J. H.; Robertson, C. M.; Harrington, L. E.; Jenkins, H. A.; Britten, J. F. *Organometallics* **2009**, *28*, 1891.
(27) Cruz, C. A.; Emslie, D. J. H.; Harrington, L. E.; Britten, J. F. *Organometallics* **2007**, *27*, 15.
(28) Cruz, C. A.; Emslie, D. J. H.; Harrington, L. E.; Britten, J. F.; Robertson, C. M. *Organometallics* **2007**, *26*, 692.
(29) Jantunen, K. C.; Batchelor, R. J.; Leznoff, D. B. *Organometallics* **2004**, *23*, 2186.
(30) Hayes, C. E.; Leznoff, D. B. *Organometallics* **2010**, *29*, 767.
(31) Cummins, C. C. *Chem. Commun.* **1998**, 1777.
(32) Clark, D. L.; Sattelberger, A. P.; Bott, S. G.; Vrtis, R. N. *Inorg. Chem.* **1989**, *28*, 1771.
(33) Avens, L. R.; Bott, S. G.; Clark, D. L.; Sattelberger, A. P.; Watkin, J. G.; Zwick, B. D. *Inorg. Chem.* **1994**, *33*, 2248.
(34) Brennan, J. G.; Andersen, R. A. *J. Am. Chem. Soc.* **1985**, *107*, 514.
(35) Avdeef, A.; Raymond, K. N.; Hodgson, K. O.; Zalkin, A. *Inorg. Chem.* **1972**, *11*, 1083.
(36) Burns, J. H. *J. Organomet. Chem.* **1974**, *69*, 225.
(37) Baudry, D.; Bulot, E.; Charpin, P.; Ephritikhine, M.; Lance, M.; Nierlich, M.; Vigner, J. *J. Organomet. Chem.* **1989**, *371*, 155.
(38) Garbar, A. V.; Leonov, M. R.; Zakharov, L. N.; Struchkov, Y. T. *Russ. Chem. Bull.* **1996**, *45*, 451.
(39) In *Landolt-Börnstein: Numerical Data and Functional Relationships in Science and Technology*; Madelung, O., Ed.; Springer: Berlin, 1987; p 15.
(40) Hitchcock, P. B.; Lappert, M. F.; Protchenko, A. V. *J. Am. Chem. Soc.* **2001**, *123*, 189.
(41) Duff, A. W.; Jonas, K.; Goddard, R.; Kraus, H. J.; Krueger, C. *J. Am. Chem. Soc.* **1983**, *105*, 5479.
(42) La Mar, G. N.; Horrocks, W. d. W.; Holm, R. H. *NMR of paramagnetic molecules; principles and applications*; Academic Press: New York, 1973.
(43) Morris, D. E.; DaRe, R. E.; Jantunen, K. C.; Castro-Rodriguez, I.; Kiplinger, J. L. *Organometallics* **2004**, *23*, 5142.
(44) Schelter, E. J.; Yang, P.; Scott, B. L.; Thompson, J. D.; Martin, R. L.; Hay, P. J.; Morris, D. E.; Kiplinger, J. L. *Inorg. Chem.* **2007**, *46*, 7477.
(45) Cantat, T.; Graves, C. R.; Jantunen, K. C.; Burns, C. J.; Scott, B. L.; Schelter, E. J.; Morris, D. E.; Hay, P. J.; Kiplinger, J. L. *J. Am. Chem. Soc.* **2008**, *130*, 17537.
(46) Morris, D. E.; Da Re, R. E.; Jantunen, K. C.; Castro-Rodriguez, I.; Kiplinger, J. L. *Organometallics* **2004**, *23*, 5142.
(47) Lever, A. B. P. *Inorganic Electronic Spectroscopy*; Elsevier: Amsterdam, 1984; Vol. 33.
(48) Kanellakopulos, B. In *Organometallics of the f-Elements*; Marks, T. J., Fischer, R. D., Eds.; D. Reidel: Dordrecht, The Netherlands, 1979; p 1.
(49) Castro-Rodriguez, I.; Olsen, K.; Gantzel, P.; Meyer, K. *J. Am. Chem. Soc.* **2003**, *125*, 4565.
(50) Kozimor, S. A.; Bartlett, B. M.; Rinehart, J. D.; Long, J. R. *J. Am. Chem. Soc.* **2007**, *129*, 10672.
(51) Rinehart, J. D.; Harris, T. D.; Kozimor, S. A.; Bartlett, B. M.; Long, J. R. *Inorg. Chem.* **2009**, *48*, 3382.
(52) Stewart, J. L.; Andersen, R. A. *New J. Chem.* **1995**, *19*, 587.
(53) Rosen, R. K.; Andersen, R. A.; Edelstein, N. M. *J. Am. Chem. Soc.* **1990**, *112*, 4588.
(54) Brown, F. C. In *Synchrotron radiation research*; Winick, H., Doniach, S., Eds.; Plenum Press: New York, 1980; p 61.
(55) In *X-ray absorption: Principles, applications, techniques of EXAFS, SEXAFS, and XANES*; Koningsberger, D. C., Prins, R., Eds.; Wiley: New York, 1988.
(56) Kalkowski, G.; Kaindl, G.; Brewer, W. D.; Krone, W. *J. Phys. Colloq.* **1986**, *47*, 943.
(57) Bertsch, P. M.; Hunter, D. B.; Sutton, S. R.; Bajt, S.; Rivers, M. L. *Environ. Sci. Technol.* **1994**, *28*, 980.
(58) Lukens, W. W.; Allen, P. G.; Bucher, J. J.; Edelstein, N. M.; Hudson, E. A.; Shuh, D. K.; Reich, T.; Andersen, R. A. *Organometallics* **1999**, *18*, 1253.
(59) Kozimor, S. A.; Yang, P.; Batista, E. R.; Boland, K. S.; Burns, C. J.; Clark, D. L.; Conradson, S. D.; Martin, R. L.; Wilkerson, M. P.; Wolfsberg, L. E. *J. Am. Chem. Soc.* **2009**, *131*, 12125.
(60) Li, J.; Bursten, B. E. *J. Am. Chem. Soc.* **1998**, *120*, 11456.

(61) Boerrigter, P. M.; Baerends, E. J.; Snijders, J. G. *Chem. Phys.* **1988**, *122*, 357.

(62) Brennan, J. G.; Green, J. C.; Redfern, C. M. *J. Am. Chem. Soc.* **1989**, *111*, 2373.

(63) Neidig, M. L.; Clark, D. L.; Martin, R. L. *Coord. Chem. Rev.* **2013**, *257*, 394.

(64) Eichkorn, K.; Weigend, F.; Treutler, O.; Ahlrichs, R. *Theor. Chem. Acc.* **1997**, *97*, 119.

(65) Veryazov, V.; Malmqvist, P.Å.; Roos, B. O. *Int. J. Quantum Chem.* **2011**, *111*, 3329.

(66) Löwdin, P.-O. *Phys. Rev.* **1955**, *97*, 1474.

(67) Gagliardi, L.; Lindh, R.; Karlström, G. *J. Chem. Phys.* **2004**, *121*, 4494.

(68) Pangborn, A. B.; Giardello, M. A.; Grubbs, R. H.; Rosen, R. K.; Timmers, F. J. *Organometallics* **1996**, *15*, 1518.

(69) Schwindt, M. A.; Lejon, T.; Hegedus, L. S. *Organometallics* **1990**, *9*, 2814.

(70) Miura, Y.; Oka, H.; Yamano, E.; Morita, M. *J. Org. Chem.* **1997**, *62*, 1188.

(71) Ruppa, K. B. P.; Desmangles, N.; Gambarotta, S.; Yap, G.; Rheingold, A. L. *Inorg. Chem.* **1997**, *36*, 1194.

(72) Sheldrick, G. *Acta Cryst. A* **2008**, *64*, 112.

(73) Perdew, J. P.; Burke, K.; Ernzerhof, M. *Phys. Rev. Lett.* **1996**, *77*, 3865.

(74) Grimme, S. *J. Comput. Chem.* **2006**, *27*, 1787.

(75) Schafer, A.; Huber, C.; Ahlrichs, R. *J. Chem. Phys.* **1994**, *100*, 5829.

(76) Ahlrichs, R.; Bär, M.; Häser, M.; Horn, H.; Kölmel, C. *Chem. Phys. Lett.* **1989**, *162*, 165.

(77) Cao, X.; Dolg, M. *J. Mol. Struct. (THEOCHEM)* **2004**, *673*, 203.

(78) Eichkorn, K.; Treutler, O.; Öhm, H.; Häser, M.; Ahlrichs, R. *Chem. Phys. Lett.* **1995**, *240*, 283.

(79) Roos, B. O.; Taylor, P. R.; Siegbahn, P. E. M. *Chem. Phys.* **1980**, *48*, 157.

(80) Andersson, K.; Malmqvist, P.-A.; Roos, B. O. *J. Chem. Phys.* **1992**, *96*, 1218.

(81) Andersson, K.; Malmqvist, P. A.; Roos, B. O.; Sadlej, A. J.; Wolinski, K. *J. Phys. Chem.* **1990**, *94*, 5483.

(82) Aquilante, F.; De Vico, L.; Ferré, N.; Ghigo, G.; Malmqvist, P. A.; Neogrády, P.; Pedersen, T. B.; Pitoňák, M.; Reiher, M.; Roos, B. O.; Serrano-Andrés, L.; Urban, M.; Veryazov, V.; Lindh, R. *J. Comput. Chem.* **2010**, *31*, 224.

(83) Douglas, M.; Kroll, N. M. *Ann. Phys.* **1974**, *82*, 89.

(84) Hess, B. A. *Phys. Rev. A* **1986**, *33*, 3742.

(85) Roos, B.r.O.; Lindh, R.; Malmqvist, P.-Ã.k.; Veryazov, V.; Widmark, P.-O. *J. Phys. Chem. A* **2003**, *108*, 2851.

(86) Roos, B. O.; Lindh, R.; Malmqvist, P. A.; Veryazov, V.; Widmark, P.-O. *Chem. Phys. Lett.* **2005**, *409*, 295.

(87) Aquilante, F.; Gagliardi, L.; Pedersen, T. B.; Lindh, R. *J. Chem. Phys.* **2009**, *130*, 154107.

(88) Aquilante, F.; Lindh, R.; Pedersen, T. B. *J. Chem. Phys.* **2008**, *129*, 034106.

(89) Aquilante, F.; Malmqvist, P.-A.; Pedersen, T. B.; Ghosh, A.; Roos, B. O. *J. Chem. Theory Comput.* **2008**, *4*, 694.

(90) Aquilante, F.; Pedersen, T. B.; Lindh, R. *J. Chem. Phys.* **2007**, *126*, 194106.